



TECHNICAL ARTICLE

# Novel Selective Laser Printing Via Powder Bed Fusion of Ionic Liquid Harvested Iron for Martian Additive Manufacturing

Blake C. Stewart, Haley R. Doude, Shiraz Mujahid, Eric T. Fox, Jennifer E. Edmunson, Morgan B. Abney, and Hongjoo Rhee

Submitted: 15 September 2021 / Revised: 20 January 2022 / Accepted: 7 February 2022

As the race to colonize Mars continues, the need for energy efficient, low waste manufacturing techniques remains as a major hurdle. Launching building materials from Earth is not feasible logistically or financially; therefore, in-situ resource utilization (ISRU) methods are required to ensure the success and longevity of these Martian colonies. Ionic liquids (ILs) are currently studied at NASA's Marshall Space Flight Center (MSFC) as a means to harvest metallic elements from regolith oxides and meteorites. IL technology provides an energy efficient method to extracting critical manufacturing materials, such as iron (Fe), that can be used for structures, plumbing, and tools. In this study, IL-sourced Fe (IL-Fe) was used as feedstock for laser-based powder bed fusion (PBF-LB) to obtain a baseline of material characteristics for additive manufacturing. Samples were then investigated to determine microstructure, hardness, and chemical composition. IL-Fe showed potential as a feedstock for the production of metallic materials via laser-based additive manufacturing techniques.

**Keywords** additive manufacturing, powder metallurgy, ionic liquids, martian manufacturing, regolith

## 1. Introduction

Manned missions to Mars and their long term habitation on the surface remain a hot topic in space exploration. Due to the astronomical cost and logistical challenge of launching building materials to extraterrestrial bodies, ISRU technology is critical for the success, longevity, and health of the astronauts that will be stationed on the red planet. Under such circumstances,

This invited article is part of a special issue in the *Journal of Materials Engineering and Performance* entitled "Space and Aerospace Exploration Revolution: Metal Additive Manufacturing." The issue was organized by Shahrooz Nafisi, Relativity Space; Paul Gradl, NASA Marshall Space Flight Center; Douglas Hofmann, NASA Jet Propulsion Laboratory/California Institute of Technology; and Reza Ghomashchi, The University of Adelaide, Australia.

**Blake C. Stewart** and **Hongjoo Rhee**, Center for Advanced Vehicular Systems, Mississippi State University, Mississippi State, MS 39762, United States; and Department of Mechanical Engineering, Mississippi State University, Mississippi State, MS 39762, United States; **Haley R. Doude** and **Shiraz Mujahid**, Center for Advanced Vehicular Systems, Mississippi State University, Mississippi State, MS 39762, United States; **Eric T. Fox** and **Jennifer E. Edmunson**, Marshall Space Flight Center, National Aeronautics and Space Administration, Huntsville, AL 35812, United States; and **Morgan B. Abney**, Langely Research Center, National Aeronautics and Space Administration, Hampton, VA 23666, United States. Contact e-mails: bcs346@cavs.msstate.edu, haley@cavs.msstate.edu, shiraz@cavs.msstate.edu, eric.t.fox@nasa.gov, jennifer.e.edmunson@nasa.gov, morgan.b.abney@nasa.gov, hrhee@me.msstate.edu.

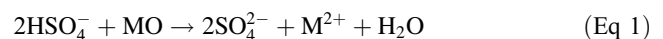
mechanical components, structural parts, and tools will be required to construct habitats utilizing the local materials.

While the Martian surface is rich in metallic elements, the regolith is composed of primarily of silicate minerals containing bound metal elements (Ref 1–6). The composition of the Martian regolith at known locations is shown in Table 1.

One of the most widely utilized building materials for terrestrial applications is ferrous alloys. Due to the significant quantity of Fe in the Martian regolith, Fe-bearing minerals could be a worthwhile material of choice for Martian manufacturing, leveraging the plethora of research on these materials on Earth. However, in order to use the Fe or other elements present in the regolith, the metal(s) must be reduced to their elemental metallic forms.

To reduce Fe oxide on Earth, a blast furnace can be used; however, this process requires extremely high temperatures and energy utilization. Indeed, there are limited energy resources on Mars, and the production of energy is demanding and expensive. Thus, a low-energy, low-waste method of reducing these metal-bearing materials into high purity elements is of utmost importance to ensure successful Martian manufacturing.

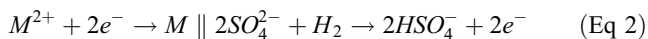
ILs are currently investigated at NASA's MSFC as a method of harvesting metallic elements from regolith and meteorites on other planetary bodies, as well as life support systems, beyond low-Earth orbit. IL technology uses liquid organic salts to dissolve the regolith minerals and recover elemental metals via electrodeposition process. The product water can also be electrolyzed to produce breathable oxygen (O<sub>2</sub>) and hydrogen gas (H<sub>2</sub>) that is used to regenerate the IL. The reactions of the IL process are shown in Eq 1 and 2 where M specifies a metal (Ref 7).



and

**Table 1. Martian Regolith composition in wt.% (Ref 1–6)**

SiO <sub>2</sub>	MnO	Fe <sub>x</sub> O <sub>y</sub>	Ni	MgO	Al <sub>2</sub> O <sub>3</sub>	CaO	Cr <sub>2</sub> O <sub>3</sub>	Cu	Zn	Other
48	0.3	15	0.02	6	12	8	0.2	.058	0.17	Bal.
±6	±0.1	±4	±0.01	±2	±5	±2	±0.2	±0.007	±0.01	



ILs can be readily modified to harvest different elements for specific applications, but Fe is the largest scale product thus far at 1-2 g Fe/day at MSFC (Ref 7). Due the range of uses and the low energy utilization of ILs, the use of this technology for Fe production in Martian manufacturing is promising. Depending on the application, IL-Fe could potentially be used without further alloying.

IL-Fe is of interest in an additive manufacturing (AM) environment. Traditional manufacturing methods such as casting, rolling, forging, etc., are well understood, but these techniques also require significant energy input. AM allows for the production of complex geometry without machining or post-processing while also reaching the low waste and low energy targets. For a Martian environment, any post-processing is undesirable due to the limited energy resources that will be available on the surface. IL-Fe could potentially be used as-produced or with minimal grinding or milling, as well as be used without the need for further alloying due to the unique chemical composition of the material. In this paper, the use of IL-Fe as feedstock for PBF-LB printing was investigated to establish a baseline of material characteristics in an AM environment.

## 2. Materials and Methods

### 2.1 Feedstock Material

The composition of the IL-Fe was found with ICP-MS (inductively coupled plasma mass spectrometry) analysis by MSFC researchers. The IL-Fe samples manufactured and provided by NASA were removed from the cell, dried under a vacuum, and stored in an argon (Ar) or nitrogen gas (N<sub>2</sub>) environment prior to being packaged in air-tight containers and shipped to the facility at Mississippi State University. The morphologies of as-received and as-ground IL-Fe produced by MSFC are shown in Fig. 1.

Due to the irregular sizing and flaky morphology of the IL-Fe, some grinding was required to print with this material. Approximately 22.5 g of the IL-Fe was available for this study. The powder was ground multiple times to ensure a semi-regular powder with no flakes using a small coffee grinder. The grinder and the IL-Fe were loaded into an oxygen free glovebox to prevent further oxidation of the material prior to printing.

Three samples, approximately 6 g each, of the ground powder were tested for estimated powder size distribution with a Horiba (Kyoto, Japan) LA-950 laser scattering particle size distribution analyzer. Powder morphology was investigated with a JEOL (Peabody, MA, USA) 6500 scanning electron microscope (SEM). The powder sample was poured onto a

12.7-mm-aluminum (Al) specimen mount with carbon (C) tape with excess powder removed.

To determine the allotropy of the IL-Fe powder, x-ray diffraction (XRD) was performed using a Rigaku (Tokyo, Japan) Ultima III x-ray diffractometer using the Diffracted Beam Monochromator (DBM) to reduce noise. Samples were mounted in 0.5-mm-glass slides and analyzed using a copper K- $\alpha$  wavelength with a scan speed of 0.125 degrees/minute.

### 2.2 Laser Sintering

A Renishaw (Wotton-under-Edge, UK) AM400 laser powder bed fusion (PBF-LB) AM machine was used to print the test specimens with the reduced build volume (RBV) build plate and without the wiper. The substrate used for this experimentation was EN 10130 1.0330 mild steel. The printing parameters are shown in Table 2. The value for energy input, Q, was found with Eq 3 (Ref 8).

$$Q = \frac{\text{Laser Power (Exposure Time / Hatch Space} \times \text{Point Distance)}}{\text{Layer Thickness}} \quad (\text{Eq 3})$$

Due to the low quantity available and the morphology of the powder, the layer was achieved by obtained by first printing a guide border and series of posts on the substrate at 50- $\mu$ m-thickness, pouring the IL-Fe powder onto the build plate, and spreading the powder with a tamping dowel. The powder prepared on the build plate prior to printing is shown in Fig. 2. This process was repeated to print a second set of disks that were five layers thick.

### 2.3 Chemical Composition

Chemical compositions of the printed IL-Fe plates were obtained using energy dispersive x-ray spectroscopy (EDS) during the SEM morphology analysis. EDS mapping of Fe and oxygen (O) of the deposited material on the substrate was also completed.

### 2.4 Microstructure

Transverse cuts through the printed samples and the build plate were made to create half cylinders for microstructural evaluation. After polishing the cut faces up to a 0.04- $\mu$ m-silica suspension, a 2% Nital etchant was used to reveal microstructural phases. Micrographs of the printed disks were imaged with a Zeiss (Oberkochen, Germany) Axiovert 200M optical microscope. Deposition thickness was measured using ImageJ software.

### 2.5 XRD

To further analyze the deposited material, XRD was performed on the printed IL-Fe disk processed under a laser

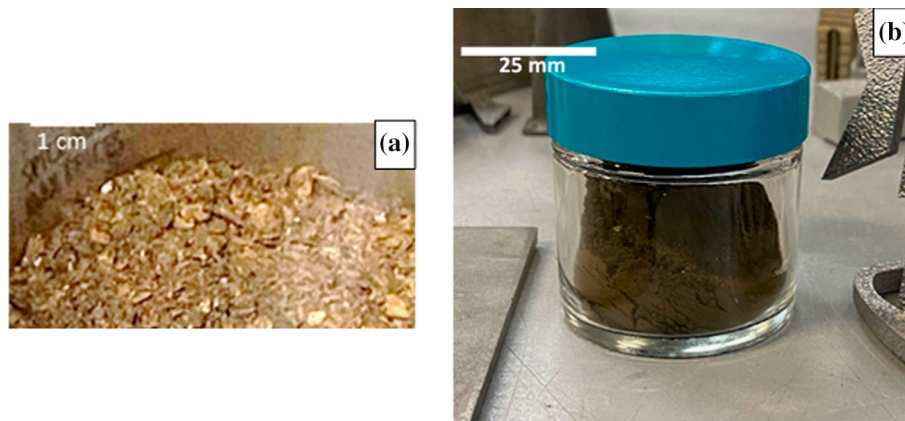


**Fig. 1.** IL-Fe produced by MSFC. (a) As-received, (b) as-ground at MSU facility

**Table 2. Printing parameters for PBF-LB of IL Fe**

Layer thickness, $\mu\text{m}$	Laser power, W	Point distance, $\mu\text{m}$	Exposure time, $\mu\text{s}$	Velocity, mm/s	Hatch space, mm	Q, J/mm
50	200	65	110	590.91	0.060	112.821
	250					141.026
	300					169.231

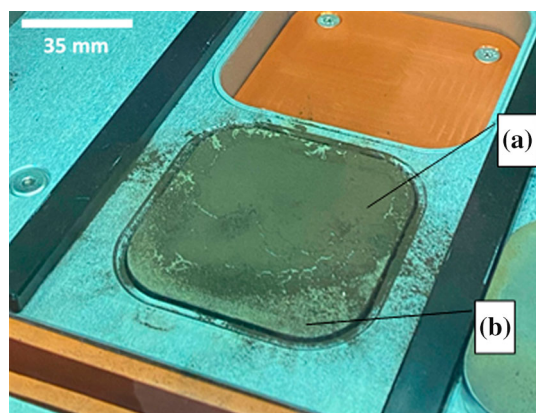


**Fig. 2.** IL-Fe powder prepared on the build plate before printing. (a) IL-Fe feedstock (brown/red colored powder) and (b) mild steel substrate (gray plate)

power of 300 W. The same Rigaku Ultima III x-ray diffractometer was used without the DBM. The sample was analyzed with a scan speed of 0.05 degrees/minute. Additionally, the build plate alone was scanned with the same parameters in order to determine if XRD results from the IL-Fe plate showed additional peaks from the build plate, and a subtraction technique was used to determine which peaks were indicative of the deposited IL-Fe.

### 2.6 Hardness Testing

A Leco (St. Joseph, MI, USA) LM-300AT Vickers micro-hardness tester was used for testing with an applied load of 10 gf on the cut face of each sample from microstructural investigation. The samples were polished with a 0.04- $\mu\text{m}$ -silica suspension prior to hardness testing. The indentations were

imaged with the Axiovert microscope followed by measurements using ImageJ software to determine hardness.

## 3. Results and Discussion

### 3.1 Feedstock Material

The chemical composition of the metallic IL-Fe is shown in Table 3.

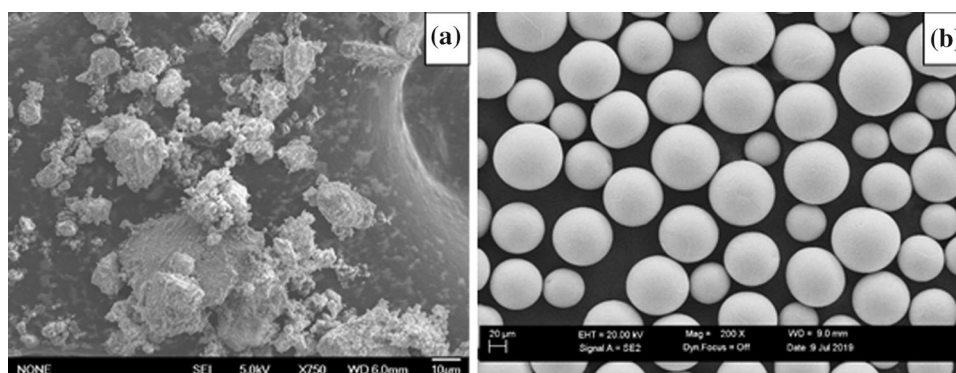
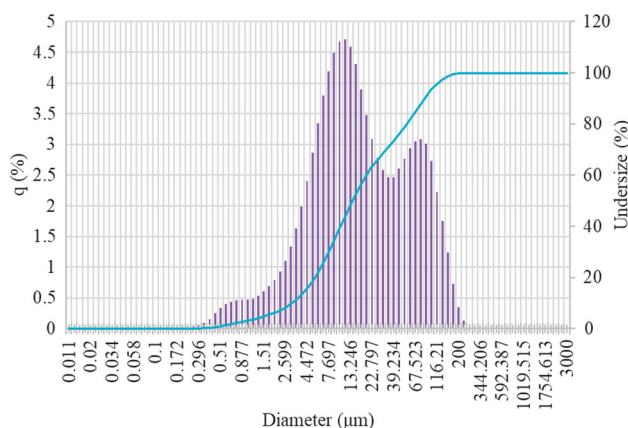
The metallic composition of the IL-Fe accounted for  $60.83 \pm 9$  wt.% of the total sample mass. Based on the visible surface oxidation of the IL-Fe flakes, the remaining  $39.17 \pm 9$  wt.% is predominantly O in the form of metal oxides. These metal oxides present are not undigested regolith components; the metals are oxidized in the electrochemical cell that is used to harvest the Fe as there is the simultaneous action of electrolyzing water in the cell. An SEM image of the IL-Fe powder is shown in Fig. 3.

SEM imaging of the ground IL-Fe powder revealed an irregular, non-spherical geometry as expected due to the production and post-processing techniques used for this study. Traditionally used AM powders would be spheroidized, such as shown in Fig. 3(b), to enhance flow behavior (Ref 9). However, Rogalsky et al. (Ref 10) showed that with adequate hopper modifications, irregular powders can be used to print components with a slight reduction in density, which could be viable for non-critical components in a Martian habitat. The powder size distribution found is shown as an average of three samples in Fig. 4.

Particle size and morphology were not investigated prior to grinding due to the large variation in sizes and shape. Future studies to investigate flow properties of ground, non-spherical IL-Fe powder could be useful and potentially negate the need for further processing of IL-Fe after grinding. However, particle

**Table 3. ICP-MS analysis results for IL-Fe (in wt.%)**

	Al	Ca	Co	Mg	Mn	Na	Ni	Si	Fe
IL-Fe (n=3)	0.07 ±0.08	0.07 ±0.06	0.05 ±0.05	1.37 ±0.2	0.28 ±0.02	0.03 ±0.02	0.08 ±0.01	0.84 ±0.09	58.04 ±9

**Fig. 3.** SEM micrographs contrasting particle morphology between (a) IL-Fe powder after grinding and (b) traditionally shaped spherical powder (Ti-6V-4Al)**Fig. 4.** Powder size distribution for ground IL-Fe powder ( $n=3$ )

size will likely need to be refined in order to obtain high density components (Ref 11).

The XRD data for the IL-Fe powder are shown in Fig. 5.

The XRD results for the IL-Fe powder show the presence of Fe and magnetite ( $\text{Fe}_3\text{O}_4$ ). The purpose of this work was to determine if the IL-Fe material could be used in the current form of production, but it is not metallic enough in nature. The formation of this oxide is not desirable for AM components made purely from IL-Fe; however, magnetite powders have been shown to be potential reinforcement for other applications such as concrete, irradiation shielding, and others (Ref 12).

During the production of IL metals, the produced material is desired to be in an elemental form or in the +2 oxidative state, in this case  $\text{Fe}^{2+}$ . This ion, when bound with oxygen, forms hematite ( $\text{Fe}_2\text{O}_3$ ). If the IL-Fe is in the form of  $\text{Fe}_2\text{O}_3$ , this could allow the material to be used for printing with Al by utilizing the exothermic thermite reaction (Ref 13). As shown by Dadbakhsh et al. (Ref 14), the use of Al and  $\text{Fe}_2\text{O}_3$  powders in PBF-LB applications can be used to reduce the laser power requirement and minimize powder bed pre-heating by utilizing

the thermite reaction in-situ and produce complex components (Ref 14,15). Higher quantities of  $\text{Fe}_2\text{O}_3$  provided significant benefits to hardness at the expense part density. Due to the limited energy resourced available on other planets, the use of  $\text{Fe}_2\text{O}_3$  IL Fe in Al could be a sufficient technique to increase production while reducing power consumption.

### 3.2 Laser Sintering

The printed disks on the build plate are shown in Fig. 6.

After printing, it was found that the single layer melting attempts were unsuccessful at depositing any appreciable IL-Fe material. However, the multilayer prints provided sound deposition layers between approximately 10 and 20  $\mu\text{m}$  of IL-Fe. Hereafter, only the multilayer prints were further investigated.

### 3.3 Chemical Composition

The chemical compositions of the powder and various printed IL-Fe plates obtained from EDS are shown in Table 4.

EDS measurements for the IL-Fe showed differences from the ICP-MS results obtained by MSFC. Traditionally, EDS quantitative measurements are not as qualitatively accurate as wavelength dispersive spectroscopy (WDS), particularly when the surface of the measured sample is not controlled, i.e., polished and flat (Ref 16). However, for the printed plates, the values found can reasonably be considered accurate as the sample was polished prior to analysis. The composition differences of the plates are not statistically significant ( $p > 0.05$ ) except for C, which is not believed to be a component of the IL Fe feedstock. With this, small quantities of C could be leached from the build plate or mounting medium, but the large amounts registered by the EDS detector are not likely.

EDS mapping of the single and multilayer prints are shown in Fig. 7 and 8, respectively. As shown in Fig. 7 and 8, the mapping further suggests that the deposited material is largely Fe and O. These images show a clear distinction of the steel

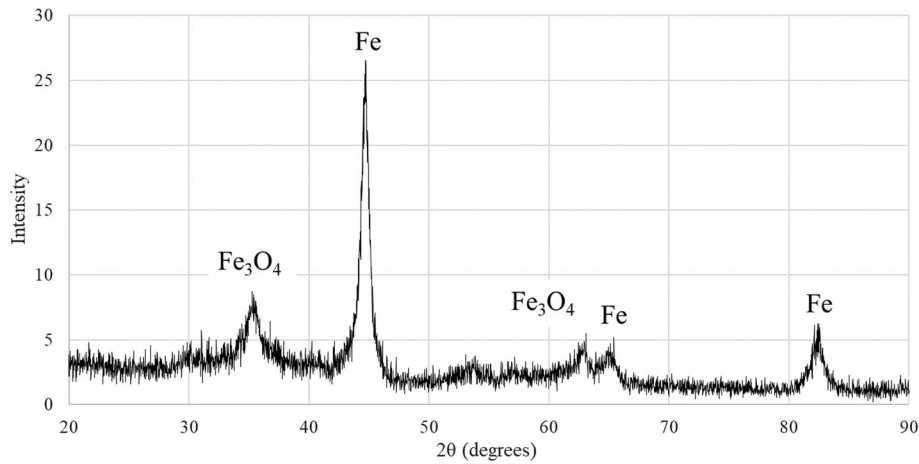


Fig. 5. XRD analysis result for IL-Fe powder

substrate and the deposited IL-Fe material by the relative concentration of Fe being significantly less in the deposited region as well as increase O content. The single layer prints were not further investigated due to the relative thickness of the deposition layer compared to that of the multilayer.

### 3.4 Microstructure

The microstructural images of the IL-Fe disks are shown in Figure 9.

When the micrographs of the deposited IL-Fe plates were investigated, it was noted that the 250 W disk showed significantly more cracking versus the 200 and 300 W sets. While only laser power was a variable for these prints, at the center of the build plate (where the 250 W multilayer print was completed) there is a 30-mm-diameter recess for the build plate elevator resulting in a 2.6-mm-thick region, whereas the remainder is 9.1-mm-thick. This leads to a possibility that the 250 W multilayer plate was embrittled by result of a greater thermal gradient when compared to the opposing disks (Ref 17,18). Figure 9(d) provides a higher magnification micrograph of the deposited IL-Fe showing the structure of the deposited material and shows weak adhesion to the build plate. While the mechanism for this delamination was not further studied, it is likely due to cracking formed during rapid cooling resulting in high residual stresses from the thermal expansion differences or a lack of chromium (Cr) enrichment available for oxide adherence (Ref 19–21). The deposition thicknesses of printed disks with respect to laser power are compared in Table 5.

Deposition measurements suggest that a greater laser input is necessary to melt and deposit IL-Fe ( $p < 0.05$ ). When compared to 316SS, the specific heat of  $\text{Fe}_3\text{O}_4$  is significantly greater (0.87 versus 0.5 J/g/°C). Along with the use of magnetite in radiation shielding (Ref 22), the deposition results showed that the laser absorptivity of  $\text{Fe}_3\text{O}_4$ , and therefore, the IL-Fe used here is likely very low.

### 3.5 XRD

The XRD analysis results for the printed plate are shown in Fig. 10.

The XRD results for the 300 W printed plate show that the deposited material is wüstite (FeO). Wüstite is a common formation in the oxide layer of steel plate, along with hematite and magnetite, where the wüstite thickness fraction will

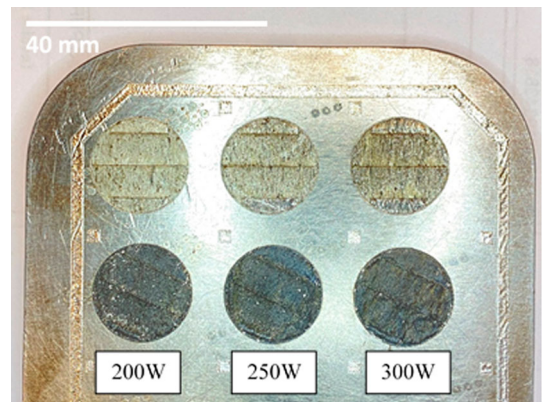


Fig. 6. Printed disks on a build plate produced in a Renishaw AM400 PBF-LB RBV. Single layer printed disks (top) and five layer printed disks (bottom)

increase with increasing cooling rate (Ref 23,24). Due to the rapid cooling rates experienced in AM components, as well as the lack of available oxygen during printing, this deposited FeO was unable to form into  $\text{Fe}_2\text{O}_3$  and  $\text{Fe}_3\text{O}_4$ . From the redox reaction of  $\text{Fe}_3\text{O}_4$ , some C from the build plate likely supplied the reactant necessary to form FeO and carbon monoxide gas during the print. This reaction is shown in Eq 4.



### 3.6 Hardness Testing

The microhardness testing results for the printed IL-Fe plates are shown in Table 6.

From the hardness testing results, there is statistical significance between the three printed samples ( $p < 0.05$ ). It was also noted that approximately 25% of indentation attempts resulted in cracking at the 10 gf applied load and 100% of the indentations with a 25 gf load. Cracking to this degree is expected of the deposited material due to remaining in an oxide form (ceramic, FeO). The 250 and 300 W plates were more consistent for hardness measurements further indicating that the IL-Fe in this form was preferable to printing with a greater laser power. The 250 W average hardness further shows a significant increase in cooling rate due to the thinner section of the build

**Table 4. Chemical compositions of IL-Fe powders and printed plates (in wt.%)**

Disk	Al	Ca	Mg	Mn	Si	Fe	O	C	Cr
IL-Fe	0.44 ±0.3	0.49 ±0.3	2.70 ±0.2	0.46 ±0	2.14 ±0.1	57.20 ±0.2	26.50 ±1	8.88 ±0.4	0
200 W	1.57 ±0.2	0.29 ±0.1	1.49 ±0.2	3.81 ±0.6	1.27 ±0.3	51.51 ±1	31.74 ±0.2	7.68 ±0.1	0.25 ±0.04
250 W	1.18 ±0.4	0.25 ±0.06	1.68 ±0.7	3.19 ±1	1.41 ±0.6	45.58 ±14	30.26 ±2	16.01 ±19	0.21 ±0
300 W	1.37 ±0.7	0.30 ±0.04	2.03 ±0.9	3.97 ±0.7	1.04 ±0.4	47.91 ±8	31.49 ±0.9	11.44 ±9	0.26 ±0

(italicized values not found by ICP-MS)

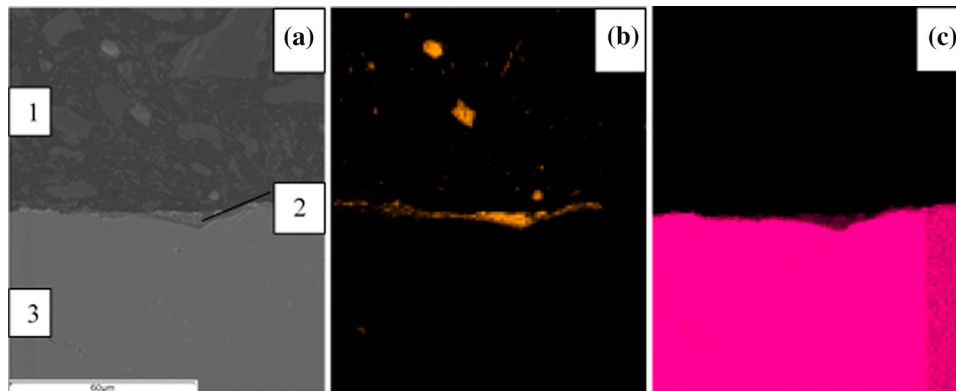
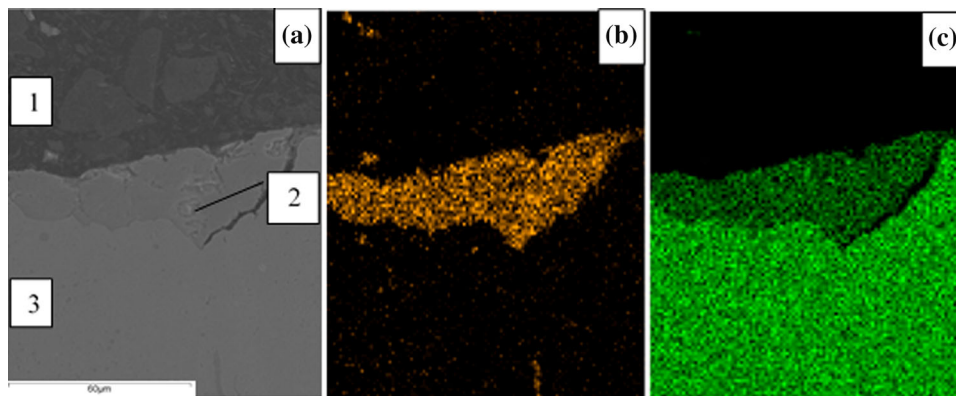
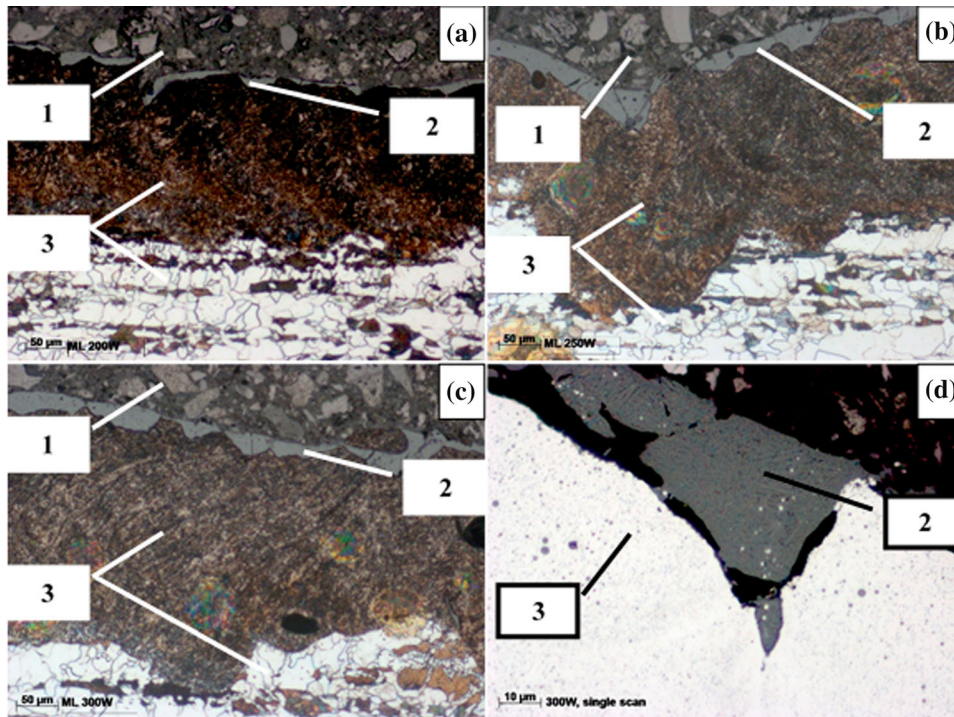
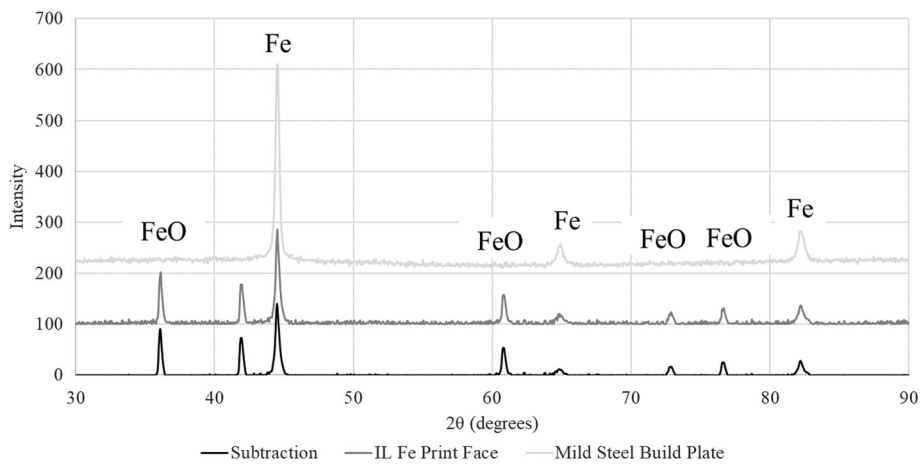
**Fig. 7.** EDS mapping of Fe and O for deposited IL-Fe (300W single layer) on steel substrate. (1) Mounting medium, (2) deposited IL-Fe, (3) steel substrate. (a) Electron image, (b) O map, (c) Fe map**Fig. 8.** EDS mapping of Fe and O for deposited IL-Fe (300W multilayer) on steel substrate. (1) Mounting medium, (2) deposited IL-Fe, (3) steel substrate. (a) Electron image, (b) O map, (c) Fe map

plate. If further investigation requires minimal material used and thin plates are printed similar to this this work, only areas that meet critical build plate thickness must be used to prevent the increased thermal gradient as seen for the 250 W plate at the

center of the substrate used here (Ref 18). Overall, hardness results confirm that the IL-Fe, in the form used here, favors higher laser powers as shown by the reduced variance of the two higher wattage parameter sets.



**Fig. 9.** Microstructural images of deposited IL-Fe disks processed under laser powers of (a) 200 W, (b) 250 W, and (c-d) 300 W. (1) Polyfast mounting medium, (2) deposited IL-Fe, and (3) mild steel substrate



**Fig. 10.** XRD data for the 300 W IL-Fe disk on build plate, build plate alone, and subtraction method

**Table 5. Deposition thickness measurements for IL-Fe plates ( $n=15$ )**

Disk (processed with a laser power of)	Measured thickness, $\mu\text{m}$
200 W	$9.1 \pm 4$
250 W	$16.4 \pm 8$
300 W	$21.0 \pm 7$

**Table 6. Vickers microhardness results of IL-Fe plates ( $n=3$ )**

Disk (processed with a laser power of)	VHN <sub>10</sub>
200 W	$666 \pm 144$
250 W	$845 \pm 24$
300 W	$533 \pm 77$

## 4. Conclusions

There exist multiple logistical challenges for producing the materials required to develop a habitable environment on the Martian surface for humankind. Traditional Fe-manufacturing approaches used on Earth are not feasible due to the lack of available energy and tooling necessary to develop large casting facilities. Post-processing capabilities are also limited due to the amount of heat and work required to produce steel alloys. Furthermore, for AM processes, there are added constraints of sourcing Fe from another planet to build components potentially without the resources required to produce spheroidized powders or other equipment used terrestrially.

Fe sourced from the IL harvesting process at MSFC was used as feedstock for PBF-LB and was printed into single and five layer disks. Microstructural, chemical, allotropic, and mechanical investigations were carried out on the resultant multilayer builds, and viable deposition can be produced using a commercially available AM method. In the current state of production, however, it is shown that higher laser powers are likely to provide more favorable deposition and properties of an IL-Fe component. The IL-Fe feedstock results, when compared to those of traditional sources, suggest that advancements should be made in feedstock production by controlling powder morphology and the reduction of  $\text{Fe}_3\text{O}_4$ , as well as larger scale production to allow for proper powder dispersion capabilities during AM investigations. However, alternative uses for oxidized material are also available. As-ground IL-Fe flow properties could be investigated in the future to advance the viability of producing IL-Fe AM components if a spheroidization operation is not feasible on the Martian surface. While the IL-Fe utilized for this study could not be used to define a baseline of parameters for PBF-LB, the presented experimental work here highlights the necessary steps that will provide a viable feedstock made from IL-Fe for AM of metallic components on the Martian surface. Currently, there is a lack of published work on using IL-Fe as feedstock for AM in an extraterrestrial setting; therefore, this is certainly a topic to be explored further. Overall, these investigations show that IL-Fe could be a promising feedstock material for AM on the Martian surface, with some limitations and that significant improvements in material manufacturing and processing are required.

## Acknowledgments

The authors would like to thank the staff of Marshall Space Flight's EM22 department for providing the raw material used in this document. Additionally, we thank MSFC and the Center for Advanced Vehicular Systems for the funding of this project under Cont. No. 80NSSC20M0239 that made this research possible.

## Funding

The authors would like to thank NASA's Marshall Space Flight Center [NASA Cont.: 80NSSC20M0239] and the Center for Advanced Vehicular Systems for their funding which made this research possible.

## Conflict of interest

The authors declare that there is no conflict of interest regarding the publication of this paper.

## References

1. A. Yen, R. Gellert, B. Clark, D. Ming, P. King, M. Schmidt, L. Leshin, R. Morris, S. Squyres, and J. Campbell, "Evidence for a Global Martian Soil Composition Extends to Gale Crater," (The Woodlands, TX), 2013, <https://ntrs.nasa.gov/citations/20130009717>
2. R. V. Morris, D. W. Ming, R. Gellert, D. T. Vaniman, D. L. Bish, D. F. Blake, S. J. Chipera, S. M. Morrison, R. T. Downs, E. B. Rampe, A. H. Treiman, A. S. Yen, C. N. Achilles, P. D. Archer, T. F. Bristow, P. Cavanaugh, K. Fenrdich, J. A. Crisp, D. J. Des Marais, J. D. Farmer, J. P. Grotzinger, P. R. Mahaffy, A. C. McAdam, and J. M. Morookian, "Update on the Chemical Composition of Crystalline, Smectite, and Amorphous Components for Rocknest Soil and John Klein and Cumberland Mudstone Drill Fines at Gale Crater Mars," (The Woodlands, TX), 2015, <https://ntrs.nasa.gov/citations/20150001942>
3. M. J. Rutherford, M. Minitti, and C. M. Weitz, "Compositions of Mars Rocks: SNC Meteorites, Differentiates, and Soils," 1999, p 92–93, <https://ntrs.nasa.gov/citations/20000012732>
4. Gregory H. Peters, William Abbey, Gregory H. Bearman, Gregory S. Mungas, J. Anthony Smith, Robert C. Anderson, Susanne Douglas, and Luther W. Beegle, Mojave Mars Simulant—Characterization of a New Geologic Mars Analog, Icarus, 2008, **197**(2), p 470–479
5. C.C. Allen, K.M. Jager, R.V. Morris, D.J. Lindstrom and J.P. Lockwood, Martian Soil Simulant Available for Scientific, Educational Study, *EOS Trans. Am. Geophys. Union*, 1998, **79**(34), p 405–412
6. Carlton C. Allen, Richard V. Morris, David J. Lindstrom, Marilyn M. Lindstrom, and John P. Lockwood, "JSC Mars-1: Martian Soil Simulant," 1997
7. L.J. Karr, P.A. Curreri, G.S. Thornton, K.E. Depew, J.M. Vankeuren, M. Regelman, E.T. Fox, M.J. Marone, D.N. Donovan, and M.S. Paley, "Ionic Liquid Facilitated Recovery of Metals and Oxygen from Regolith," (Orlando, FL), 2018, <https://ntrs.nasa.gov/citations/2018006392>. Accessed 21 July 2021
8. J.A. Cherry, H.M. Davies, S. Mehmood, N.P. Lavery, S.G.R. Brown and J. Sienz, Investigation into the Effect of Process Parameters on Microstructural and Physical Properties of 316L Stainless Steel Parts by Selective Laser Melting, *Int. J. Adv. Manuf. Technol.*, 2015, **76**(5–8), p 869–879
9. A. Strondl, O. Lyckfeldt, H. Brodin and U. Ackelid, Characterization and Control of Powder Properties for Additive Manufacturing, *JOM*, 2015, **67**(3), p 549–554
10. A. Rogalsky, I. Rishmawi, L. Brock and M. Vlasea, Low Cost Irregular Feed Stock for Laser Powder Bed Fusion, *J. Manuf. Process.*, 2018, **35**, p 446–456
11. Y. Bai, G. Wagner and C.B. Williams, Effect of Particle Size Distribution on Powder Packing and Sintering in Binder Jetting Additive Manufacturing of Metals, *J. Manuf. Sci. Eng.*, 2017 <https://doi.org/10.1115/1.4036640>
12. J.J. Restrepo and H.A. Colorado, Additive Manufacturing of Composites Made of Epoxy Resin with Magnetite Particles Fabricated with the Direct Ink Writing Technique, *J. Compos. Mater.*, 2020, **54**(5), p 647–657
13. R.-H. Fan, H.-L. Lü, K.-N. Sun, W.-X. Wang and X.-B. Yi, Kinetics of Thermite Reaction in Al-Fe<sub>2</sub>O<sub>3</sub> System, *Thermochim. Acta*, 2006, **440**(2), p 129–131
14. S. Dadbakhsh, L. Hao, P.G.E. Jerrard and D.Z. Zhang, Experimental Investigation on Selective Laser Melting Behaviour and Processing Windows of in Situ Reacted Al/Fe<sub>2</sub>O<sub>3</sub> Powder Mixture, *Powder Technol.*, 2012, **231**, p 112–121
15. S. Dadbakhsh and L. Hao, Effect of Hot Isostatic Pressing (HIP) on Al Composite Parts Made from Laser Consolidated Al/Fe<sub>2</sub>O<sub>3</sub> Powder Mixtures, *J. Mater. Process. Technol.*, 2012, **212**(11), p 2474–2483
16. D.E. Newbury and N.W.M. Ritchie, Performing Elemental Microanalysis with High Accuracy and High Precision by Scanning Electron

- Microscopy/Silicon Drift Detector Energy-Dispersive x-Ray Spectrometry (SEM/SDD-EDS), *J. Mater. Sci.*, 2015, **50**(2), p 493–518
17. I. Polozov, V. Sufiarov, A. Kantuykov, N. Razumov, I. Goncharov, T. Makhmutov, A. Silin, A. Kim, K. Starikov, A. Shamshurin and A. Popovich, Microstructure, Densification, and Mechanical Properties of Titanium Intermetallic Alloy Manufactured by Laser Powder Bed Fusion Additive Manufacturing with High-Temperature Preheating Using Gas Atomized and Mechanically Alloyed Plasma Spheroidized Powders, *Addit. Manuf.*, 2020, **34**, p 101374
  18. N. Shen and K. Chou, “Numerical Thermal Analysis in Electron Beam Additive Manufacturing with Preheating Effects,” In: *Proceedings of the 23rd solid freeform fabrication symposium*, (Austin, TX), 2012, p 774–784
  19. Wengai Yang, “The Structure and Properties of Mill Scale in Relation to Easy Removal,” (Sheffield, England), University of Sheffield, 2001, <https://etheses.whiterose.ac.uk/15090/>
  20. Daryoush Ahmadi, “Oxide Scales Behavior During Descaling and Hot Rolling,” (Sheffield, England), University of Sheffield, 2019, <https://etheses.whiterose.ac.uk/27100/>
  21. J. Shi and J. Ming, Influence of Mill Scale and Rust Layer on the Corrosion Resistance of Low-Alloy Steel in Simulated Concrete Pore Solution, *Int. J. Miner. Metall. Mater.*, 2017, **24**(1), p 64–74
  22. E. Creutz and K. Downes, Magnetite Concrete for Radiation Shielding, *J. Appl. Phys.*, 1949, **20**(12), p 1236–1240
  23. R.Y. Chen and W.Y.D. Yuen, A Study of the Scale Structure of Hot-Rolled Steel Strip by Simulated Coiling and Cooling, *Oxid. Met.*, 2000, **53**, p 539–560
  24. R.Y. Chen and W.Y.D. Yuen, Oxide-Scale Structures Formed on Commercial Hot-Rolled Steel Strip and Their Formation Mechanisms, *Oxid. Met.*, 2001, **56**, p 89–118

**Publisher's Note** Springer Nature remains neutral with regard to jurisdictional claims in published maps and institutional affiliations.